Proceedings of ASME FEDSM'00
ASME 2000 Fluids Engineering Division Summer Meeting
Boston, Massachusetts, June 11-15, 2000

FEDSM2000-11144

LARGE-EDDY SIMULATION OF PARTICLE-LADEN ROTATING CHANNEL FLOW

Yingkang Pan, Toshitsugu Tanaka and Yutaka Tsuji
Department of Mechanical Engineering
Osaka University, Suita 565-0871, JAPAN
E-mail: pan@mupf., tanaka@, tsuji@ +mech.eng.osaka-u.ac.jp

ABSTRACT

Particle transports in fully-developed turbulent rotating channel flows have been investigated using the large eddy simulations (LES) of the incompressible Navier-Stokes equations based on the finite-difference technique. Lycopodium particles with diameter 28 μm were traced using the deterministic method via inter-particle collisions and particle feedback.

Simulation results showed that particle accumulations in the region near the unstable surface were detected due to system rotation, especially at high rotating speeds; the inter-particle collisions occurred frequently near the unstable surface and then severely affected the particle dynamics although the particle volume fraction was very low $O(10^{-5})$. From the present results, it is also seen that the finite-sized particles attenuate the contribution from the Coriolis forces to the turbulence and the total turbulent kinetic energy of the fluid, especially near the walls.

INTRODUCTION

Particle-laden flow in the rotating channel is an important phenomenon in many industrial fields. In such a rotating system, particle's trajectories are much affected by the Coriolis and centrifugal forces besides buoyancy due to the difference in densities of the two phases, so that they considerably deviate from the streamlines of the carrier fluid.

In the single-phase flow, Bradshaw (1969) pointed out the similarity between rotation, streamline curvature, and thermal stratification on turbulent flows. In all three cases, the body force has either a stabilizing or destabilizing effect on the flow depending on its interaction with the driving mechanism. Two important effects of rotation on a turbulent channel flow are the stabilization/destabilization of turbulence on walls normal to the axis of rotation and the generation of spanwise roll cells. In earlier numerical practice, turbulence modeling based on Reynolds equations was used to the rotational effects, namely, mixing length model (Johnston *et al.*, 1972), one-equation model (Koyama *et al*., 1979), and two-equation model (Howard *et al*., 1980). A successful application of second-moment closures to rotating turbulent shear flows was reported by Launder *et al*. (1987). Accompanying the development of the supercomputer, the direct and large-eddy simulations of turbulent rotating shear flows in the fruitful way are possible to be conducted, and thereby promote our understanding of the influences of rotation on the turbulence. The large-eddy simulations (LES) of fully developed rotating channel flows were reported by Kim (1983), Bardina *et al*. (1985), Miyake and Kajishima (1986), Tafti and Vanka (1991), Cambon *et al*. (1994), and Piomelli and Liu (1995), respectively. The direct numerical simulations (DNS) of rotating channel flows at low Reynolds number were conducted by Kristoffersen and Andersson (1993). Previous LES and DNS on rotating shear flows also reproduced many of the experimentally observed effects of the Coriolis forces on the mean flow and the turbulence.

Rouson and Eaton (1994) performed the DNS of particle-laden turbulent channel flows and found that heavy particles tend to disperse uniformly and light particles form clusters. Wang and Squires (1996) conducted the LES with a Lagrangian dynamic eddy viscosity model of particle-laden turbulent channel flows. Their results were in good agreement with the DNS of Rouson and Eaton (1994) and reasonable agreement with experimental measurements of Fessler *et al*. (1994). Yamamoto *et al*. (1998) applied the LES considering the inter-particle collisions and got that the collision statistics is considerable as the particle's concentration becomes higher.

There exist few investigations about particle-laden flows in the rotating channels. The group of Tabakoff (1984) had performed experimental and analytical investigations concerning the effects of the presence of solid particles on the performance of turbomachines. They had not considered the

inter-particle collisions and the effects from the particles to the turbulence. There are two objectives of the present work. First one is to investigate the particle statistics in a rotating channel flow; the other is to account for the effects of particles to the turbulence.

SIMULATION OVERVIEW

Fluid field

Figure 1 illustrates the coordinate system used to write the equations of motion. Here *x* (x_1) is the streamwise direction, *y* (x_2) is the wall-normal direction, and *z* (x_3) is the spanwise direction, respectively. Also, *u* (u_1) is the streamwise velocity, *v* (u_2) is the velocity in the wall-normal direction, and *w* (u_3) is the velocity in the spanwise direction.

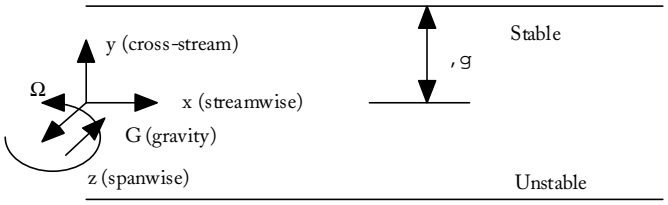

Fig. 1 Flow geometry and coordinate system

The turbulent flow in a rotating channel was calculated using the LES of the incompressible Navier-Stokes equations. In large-eddy simulations the flow variables are decomposed into a large scale (or resolved) component, denoted by an overbar, and a subgrid scale component. The equations governing transport of the large eddies obtained by filtering the continuity and Navier-Stokes equations, which can be expressed in the following forms

$$\frac{\partial \overline{u}_i}{\partial t} = 0 \tag{1}$$

$$\frac{\partial \overline{u}_i}{\partial t} + \frac{\partial}{\partial x_j}\left(\overline{u}_i \overline{u}_j\right) = -\frac{\partial \overline{p}_{eff}}{\partial x_i} - \frac{\partial \tau_{ij}}{\partial x_j} + \frac{1}{\mathrm{Re}_\tau}\frac{\partial^2 \overline{u}_i}{\partial x_j \partial x_j} + 2\varepsilon_{ij3} Ro_\tau \overline{u}_j + F_{pi} + 2\delta_{i1} \tag{2}$$

where δ_{ij} is the Kronecker delta symbol, ε_{ijk} is the Levi-Civita's alternating tensor. The last term in the right hand side in Eq. (2) is the dimensionless, gross downstream pressure gradient which would maintain a steady flow against the equilibrium, long term wall friction which produced by both boundaries. The 4th term in the right hand side in Eq. (2) is the Coriolis force experienced by a fluid element resulting from system rotation. The centrifugal force is conservative in nature and can be combined with the pressure gradient term. F_{pi} is the reaction of fluid force on particles contains in a unit mass of fluid element.

Equation (2) is nondimensionalized by the time-averaged mean wall friction velocity ($u_\tau = \sqrt{\tau_w/\rho}$) and the channel half-width (*H*). Based on this normalization, the Reynolds number is defined as $Re_\tau = u_\tau H/\nu$, and the Rotation number is defined as $Ro_\tau = \Omega H/u_\tau$, where Ω is the angular velocity of rotation. In a stationary channel flow without rotation, friction velocities are the same on both walls of the channel, but this is not the case with rotation because of the asymmetry introduced by the Coriolis forces.

The effect of the subgrid scales on the resolved eddies in Eq. (2) is represented by SGS stress, because of lack of the effective SGS model for the particle-laden flows, so the Smagorinsky model (Deardoff, 1970) will be applied

$$\nu_{SGS} = \left(C_s \Delta_s f_s\right)^2 \left| \frac{1}{2}\left(\frac{\partial u_i}{\partial x_j} + \frac{\partial u_j}{\partial x_i} \right) \right| \tag{3}$$

where C_S is a non-dimensional empirical constant, Δ_s is the filter scale, and f_S is the damping function. The filter scale Δ_S is defined by

$$\Delta_s \equiv \sqrt[3]{\Delta_1 \Delta_2 \Delta_3} \tag{4}$$

In the present simulations, the same formulation and the same constants of the SGS model as in the single-phase flow were applied for the present gas-particle flows, because of lack of ideas of modifications due to the presence of particles. Therefore, the following value is preferred for single phase turbulent rotating channel flows.

$$C_s = 0.1 \tag{5}$$

The damping function is expressed as

$$f_s = 1 - \exp\frac{-x_2^+}{25} \tag{6}$$

x_2^+ is the non-dimensional distance from the wall defined by

$$x_2^+ = \frac{x_2 u_\tau}{\nu} \tag{7}$$

The governing equations (1) and (2) were solved numerically using the SMAC method on a staggered grid. Spatial derivatives were approximated by second-order accuracy central difference

scheme and the second-order Adams-Bashforth scheme was used for the time marching. The Poisson equation for pressure was solved using Fourier series expansions in the streamwise and spanwise directions together with tridiagonal matrix inversion.

Particle motion

Although the particle volume fraction is of the order of 10^{-5} for most particle-laden rotating channel flows, especially in turbomachines, particles will concentrate in the region near the pressure surface (unstable surface) subjected to system rotation. So, the inter-particle collisions are very important in such flows and should be considered. The effects of the particles on the flow field and turbulence structure are little known. Based on above reasons, we hope to get some detailed information in particle-laden rotating channel flows from the present LES results.

Motion of a small rigid sphere in a turbulent flow field is described by a complicated equation by Maxey and Riley (1983). If the density of the particles is much larger than that of the carrier fluid, the equation of particle motion can be simplified in the rotating frame. It can be given in the following form

$$m_p \frac{du_{pi}}{dt} = \frac{1}{2}\rho|\mathrm{u}_R|A\left[C_D u_{Ri} + C_{LR}\frac{(\mathrm{u}_R \times \omega_R)_i}{|\omega_R|}\right] + f_{LG}\delta_{i2} + m_p g\delta_{i3} + \delta_{i1} m_p \Omega^2 r + 2\varepsilon_{ij3} m_p \Omega u_j \quad (8)$$

The empirical relation for C_D (Schiller and Nauman, 1933) was employed

$$C_D = \frac{24}{\mathrm{Re}_p}\left(1 + 0.15\,\mathrm{Re}_p^{0.687}\right) \quad (9)$$

The lift coefficient C_{LR} applied is the following model (Tsuji, 1984):

$$C_{LR} = \min\left[0.5, 0.25\frac{d_p|\omega_R|}{|u_R|}\right] \quad (10)$$

The lift force was employed only in the wall-normal component with the Saffman's expression as following (Saffman, 1965)

$$f_{LG} = -1.62 d_p^2 \rho u_{Rx}\sqrt{\nu\left|\frac{\partial u_{Rx}}{\partial y}\right|}\frac{\partial u_{Rx}/\partial y}{|\partial u_{Rx}/\partial y|} \quad (11)$$

The equation of rotational motion of a particle is given by

$$I\frac{d\omega_{pi}}{dt} = -C_T\frac{1}{2}\rho\left(\frac{d_p}{2}\right)^2|\omega_R|\omega_{Ri} \quad (12)$$

where I is the moment of inertia of a particle. The right hand side of Eq. (12) is the viscous torque against the particle's rotation, which is theoretically obtained by Dennis *et al.* (1980) and Takagi (1970). C_T is the non-dimensional coefficient determined by the rotational Reynolds number $\mathrm{Re}_R = d_p^2|\omega_R|/4\nu$. Because only the velocity of the fluid at every grid point was known, so the third Lagrangian interpolation polynomial was used to obtain the fluid velocities at the positions of the particles. Particle displacements were also integrated using the second-order Adams-Bashforth scheme.

As the particle density is much larger than the fluid density so that the particle inertial response time can be expressed as

$$\tau_p = \frac{\rho_p}{\rho}\frac{d_p^2}{18\nu} \quad (13)$$

Inter-particle collision

Inter-particle collisions will take an important role to the flow field near the pressure surface in the particle-laden rotating channels due to the particle concentration. In the present situations, the particle number density is so low, so that we applied the deterministic method (Tanaka and Tsuji, 1991). It is assumed that the particle volume fraction is small enough so that binary collisions dominate in our cases. In the numerical simulations, we define a collision as an event which occurs when the distance of two particle's centers is equal to the diameter of a particle. Therefore, the collision is mainly detected by calculating the distance of two particle's centers at the specific time when two particles collide with each other. Post-collision motion of the particle is described by the equations of impulsive motion:

$$u_{pi}^* = u_{pi} + \frac{\mathbf{J}}{m_p} \quad (14)$$

$$u_{pj}^* = u_{pj} - \frac{\mathbf{J}}{m_p} \quad (15)$$

$$\omega_{pi}^* = \omega_{pi} + \frac{d_p}{2}\mathbf{n}\times\frac{\mathbf{J}}{\mathbf{I}} \quad (16)$$

$$\omega_{pj}^* = \omega_{ji} + \frac{d_p}{2}\mathbf{n}\times\frac{\mathbf{J}}{\mathbf{I}} \quad (17)$$

where $\mathbf{J}$ is the impulsive force exerting on the particle i and $\mathbf{n}$ is the normal unit vector directing from the center of the particle i to the contacting point. Post-collision parameters are indicated by stars. Base on assuming spherical particles, a constant coefficient of restitution e_p and negligible particle deformation are assumed. $\mathbf{J}$ is given by Tanaka and Tsuji (1991) in following forms:

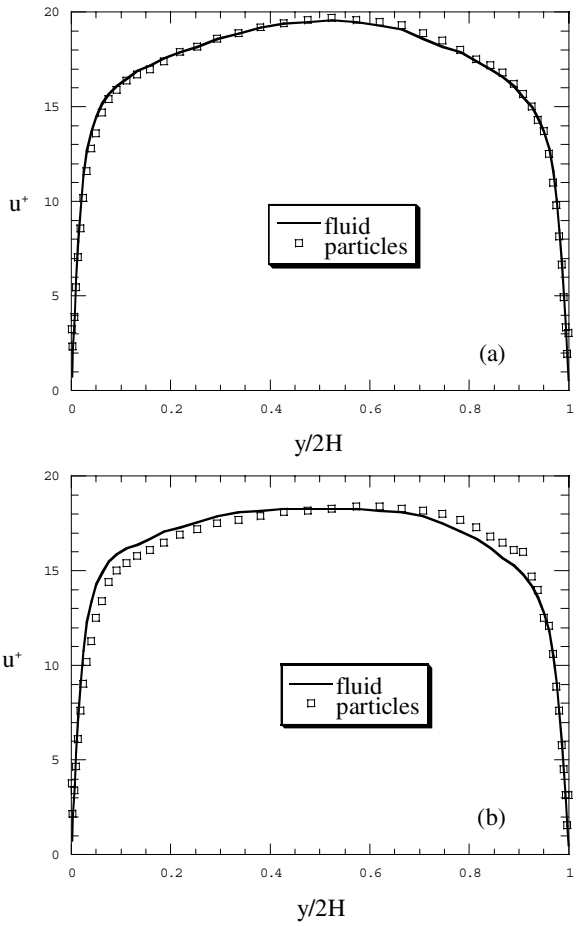

Fig.2 Mean stream velocities of the fluid and the particles, Re=250, (a) Ro=0.1,(b)Ro=0.25

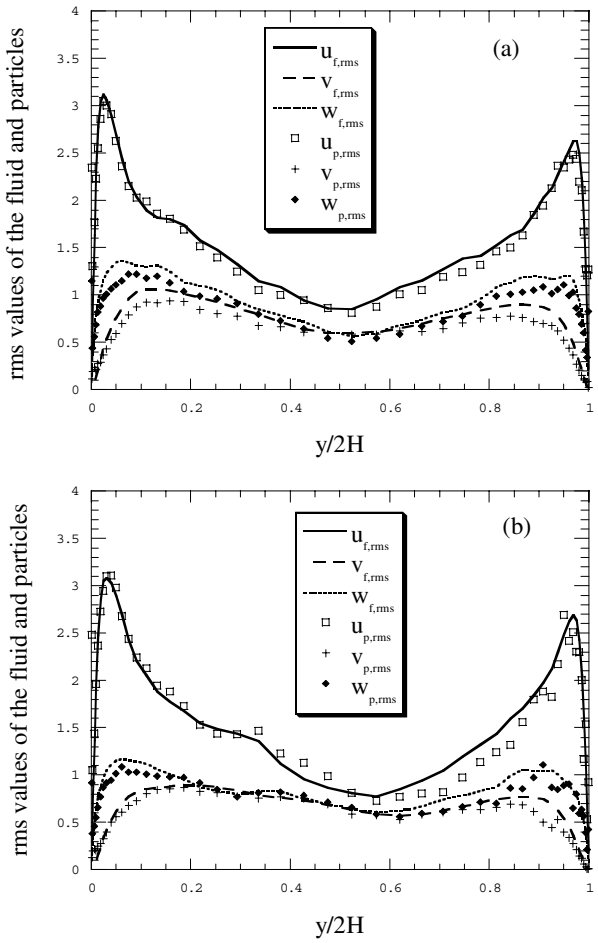

Fig.3 Root mean square values of resolved turbulent fluctuations of the fluid and the particles (a) Ro=0.1, (b)Ro=0.25

$$\mathbf{J} = J_n \mathbf{n} + J_t \mathbf{t} \tag{18}$$

$$J_t = \min\left[-\mu_p J_n, \frac{M}{7}|\mathbf{c}_s|\right] \tag{19}$$

$$J_n = (1+e_p) M \mathbf{c}\cdot\mathbf{n} \tag{20}$$

where **t** is the tangential unit vector of the slip velocity from the particle *j* to the particle *i*. e_p is the coefficient of restitution, μ_p is the coefficient of friction and *M* is equal to $m_p/2$ for inter-particle collisions and m_p for particle-wall collisions. **c** is the relative velocity of mass center, and $\boldsymbol{c}_s$ is the slip velocity at the contact point.

NUMERICAL RESULTS

The initial conditions of velocity fluctuations of the fluid and the particles were assumed by a random generator. The particle's initial velocities were assumed to be the same as the fluid velocities at the particle positions. In all the numerical experiments the calculation domain used was $9.6H \times 2.0H \times 2.4H$ in *x, y* and *z* directions, respectively. The calculation domain was divided into $64\times48\times64$ computational cells with a uniformly spaced grid in the *x* and *z* directions ($\Delta x^+ = 187.5, \Delta z^+ = 4.7$ for $Re_\tau = 250$) and a non-uniform grid distribution in the *y* direction. The Reynolds number, based on the bulk mean velocity U_m and the channel half-width *H*, was about 4950. In the present simulations a hyperbolic tan transformation is used to generate the grid in the *y* direction. To apply the periodic boundary conditions in *x* and *z* directions both the fluid and the particles, the initial inlet rotation radio is set to large enough $r_0 = 58.2H$. Properties of the dispersed phases were obtained by following the trajectories of 156,159 Lycopoidium particles with diameter $28\mu m$ with various Rotation numbers $Ro_\tau = 0.1, 0.25, 0.5, 1.0$, and 1.5, respectively. The time step used in all the calculations was 0.0002 non-dimensional time units both for the fluid and particle motions and 0.001 for the inter-particle collisions. This is much smaller than the particle relaxation time. So that the inter-

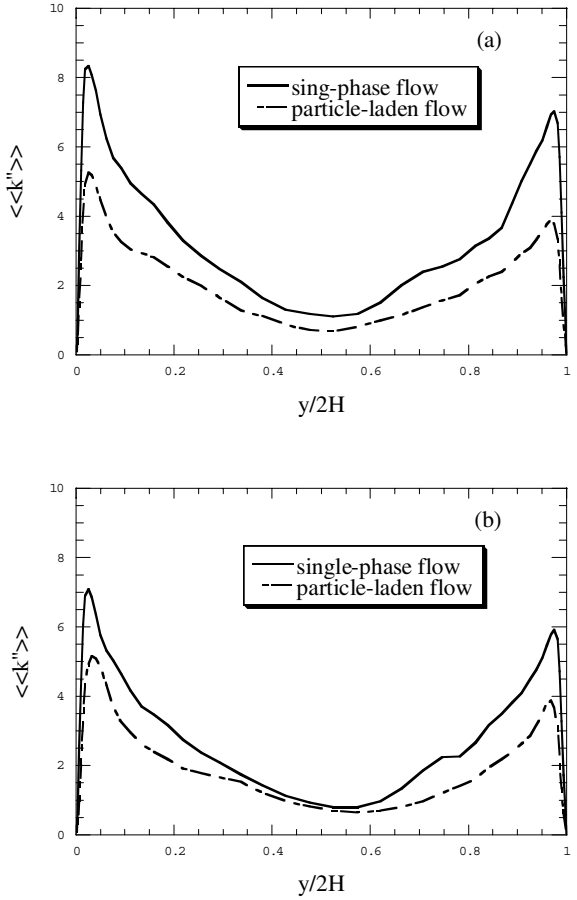

Fig.4 Distribution of total turbulent kinetic energy $<< k'' >>$ for single-phase and particle-laden flows (a) Ro=0.1, (b)Ro=0.25

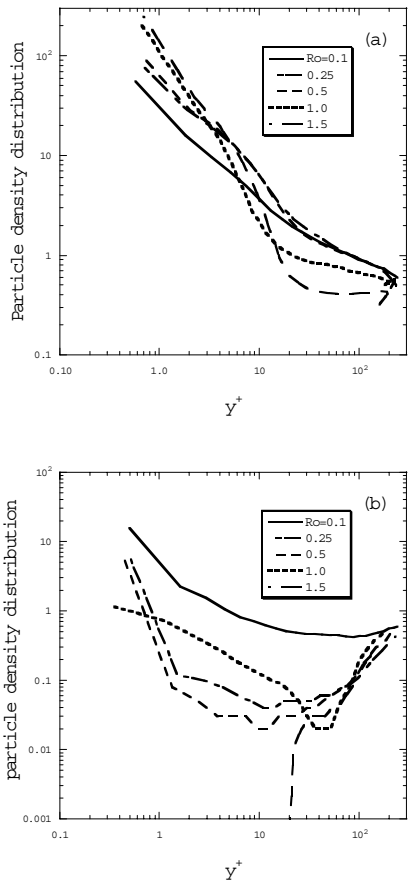

Fig.5 Particle density distribution in wall coordinates (a) near the pressure surface, (b) near the suction surface

particle collisions were examined assuming that the particle motion was linear during in the period of one time step. For getting the fully developed turbulent flow field not influenced by the initial conditions, about 12 non-dimensional time units (H/u_τ) for each case were conducted on the supercomputer SX-4 of Osaka university. Almost all parts of the program for the fluid were vectorized. It is required the CPU time of approximately 20 hours for each case. In the rest of the paper, the Reynolds number and Rotation number Re_τ, Ro_τ will be referred to as *Re* and *Ro* for notational simplicity.

The mean streamwise velocity profiles of the fluid and the particles obtained from the LES calculations are shown in Fig. 2 at different Rotation numbers Ro=0.1 and 0.25. When the Rotation number is low Ro=0.1, as expected, the mean streamwise velocity of Lycopodium particles is nearly equal to the fluid velocity (similar as the results of Wang *et al.*, 1996). When the Rotation number becomes higher Ro=0.25, the mean streamwise velocity of Lycopodium particles is different from

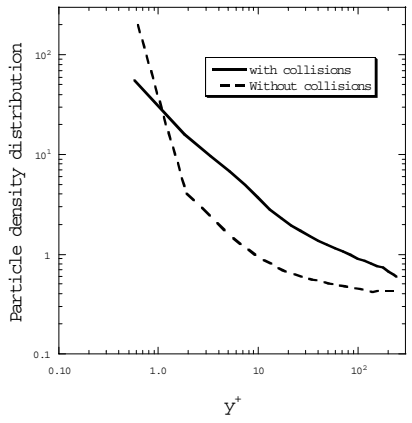

Fig. 6 Comparison of particle density distribution in wall coordinates between with and without inter-particle collisions near the pressure surface

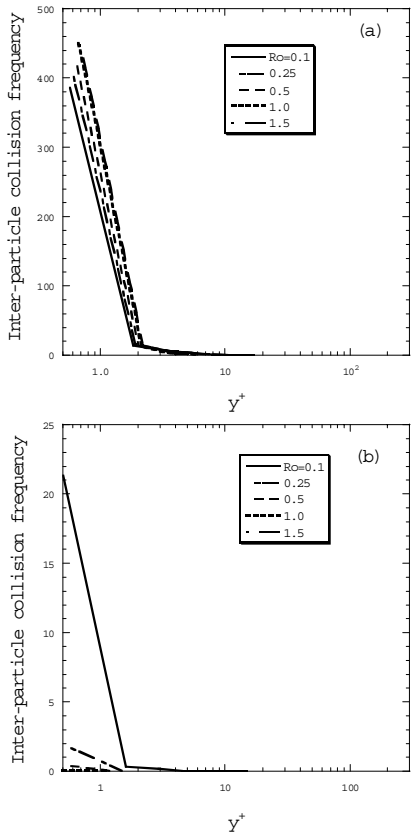

Fig.7 Inter-particle collision frequency distribution in wall coordinates,(a) near the pressure surface, (b) near the suction surface

that of the fluid due to the Coriolis and centrifugal forces, especially near the walls. Near the pressure surface, inter-particle collision frequency becomes very high because of the particle concentration, leading to be lower of particle mean streamwise velocity. Inversely, particles near the suction surface are accelerated to reach higher mean streamwise velocities due to the Coriolis and centrifugal forces.

Figure 3 shows the comparisons of the distributions of the rms values between the fluid and the particles. The rms values of the fluid and the particles are almost same in the streamwise direction. In the spanwise and wall-normal directions, rms values of the fluid are larger than those of the particles, especially in the regions near the walls. Although at low Rotation number *Ro*=0.1, the difference between the carrier fluid and the particles is obvious. The turbulent kinetic energy's distributions between the sing-phase and particle-laden flows are shown in Fig. 4. In the present simulations, the diameter of the particle is much smaller than the grid sizes, and the particle initial response time is about 1.7 *ms*. Because of existence of the Coriolis and centrifugal forces in the rotating channel, the finite-sized particle attenuates the total turbulent kinetic energy of the carrier fluid, especially in the regions near the walls.

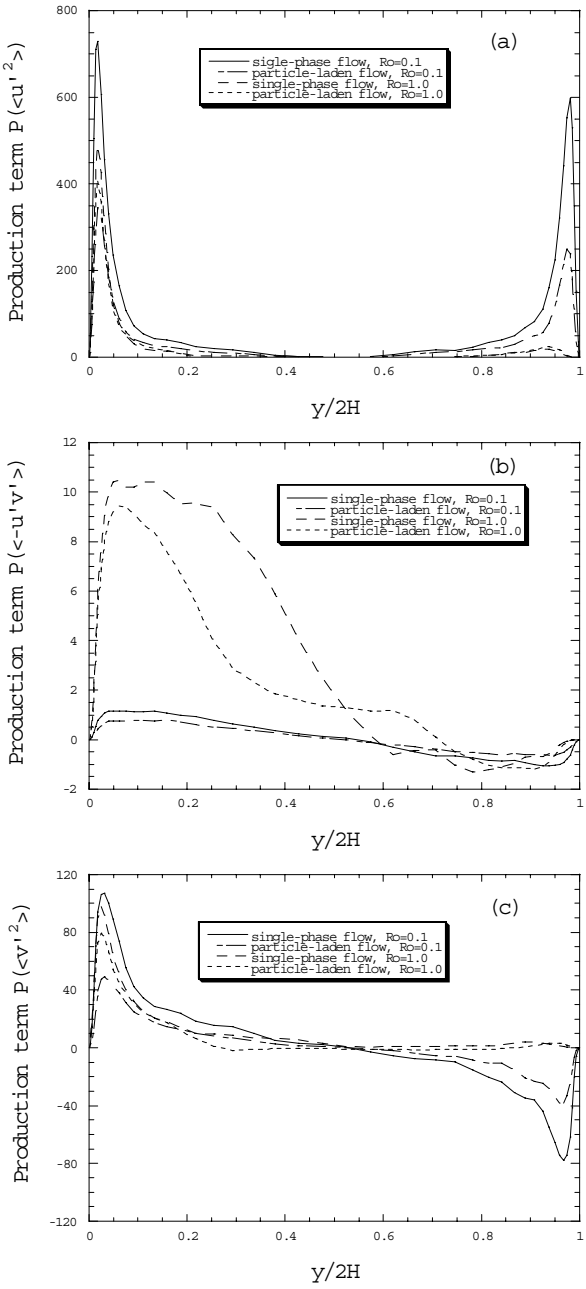

Fig. 8 Fluid's production terms distribution in global coordinates between the single-phase and particle-laden flows at Re=250 and Ro=0.1, 1.0, (a) $P\left(\left\langle u'^2 \right\rangle\right)$, (b) $P\left(\left\langle -u'v' \right\rangle\right)$, and (c) $P\left(\left\langle v'^2 \right\rangle\right)$

The particle density distributions near the walls in wall coordinates are shown in Fig. 5. From the simulation results, we can see that lots of particles will accumulate near the pressure surface, and few particles will still stay near the suction surface. When the rotation speed becomes higher *Ro*=1.5, there are almost no particles near the suction surface. It is also shown

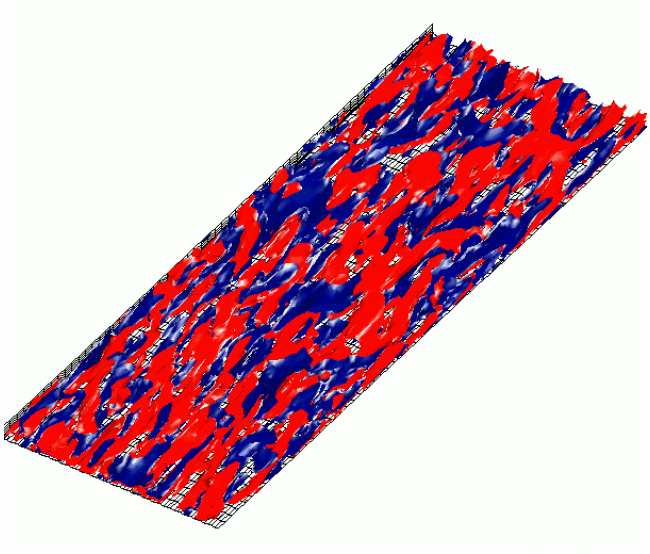

Fig. 9 Fluid's streamwise fluctuation vorticity structure of the single-phase flow at Ro=0.1 near the pressure surface

Fig. 10 Fluid's streamwise fluctuation vorticity structure of the particle-laden flow at Ro=0.1 near the pressure surface

that lots of particles will be located in the inner boundary layer $y^+<5$.

Figure 6 shows the comparison of the particle density distributions in wall coordinates between with and without inter-particle collision model near the pressure surface. From the simulation results, it is seen that the particle density distributions are very differently between with and without inter-particle collisions. Without the inter-particle collisions, more particles tend to concentrate to the pressure surface and less particles are located away from the pressure surface. So that the inter-particle collisions take a very important role in the rotating system although the particle volume fractions are very low.

Figure 7 is the simulation result of inter-particle collision frequency distributions near the pressure and suction surfaces. The inter-particle collisions will be happen frequently near the walls, especially near the pressure surface. Comparing the Fig. 5 and Fig. 7, it is seen that lots of particles concentrate in the inner boundary layer of the walls so as to cause inter-particle collisions frequently.

After neglecting the production resulting from the mean flow of the roll cells, the production terms for $\langle u'^2 \rangle$, $\langle v'^2 \rangle$, and $\langle -u'v' \rangle$ can be written as (Tafti and Vanka, 1991)

$$P\left(\langle u'^2 \rangle\right) = 2\langle -u'v' \rangle \frac{d\overline{U}}{dy} - 4Ro\langle -u'v' \rangle \tag{21}$$

$$P\left(\langle v'^2 \rangle\right) = 4Ro\langle -u'v' \rangle \tag{22}$$

$$P\left(\langle -u'v' \rangle\right) = \langle v'^2 \rangle \frac{d\overline{U}}{dy} + 2Ro\left(\langle u'^2 \rangle - \langle v'^2 \rangle\right) \tag{23}$$

the terms with *Ro* are the additional terms resulting from the action of the Coriolis forces on the turbulent fluctuations. The production for $\langle u'^2 \rangle$ can be directly related to Richardson number. Figure 8 shows the comparisons of the fluid's production terms between the single-phase and particle-laden flows at *Re*=250 and *Ro*=0.1,1.0. The whole tendencies are similar to the results of Tafti and Vanka (1991). For the particle-laden flows, the production terms are changed a little in the center area of the channel, but attenuated a lot near both walls although there is small number of particles were still located near the suction surface. The effect of the particles is attenuating the production terms for $\langle u'^2 \rangle$, $\langle v'^2 \rangle$, and $\langle -u'v' \rangle$. At the low Rotation number *Ro*=0.1, the differences of the production terms near the pressure and suction surfaces are small. At the high Rotation number *Ro*=1.0, that will becomes significant.

Figure 9 and figure 10 are the instantaneous fluid streamwise fluctuation vorticity structures of the single-phase and particle-laden flows near the pressure surface $y^+<26.5$ at 12.0 non-dimensional time units. The red (printed in grey) parts represent $\overline{\omega}_x' > 0.12u_\tau^2/\nu$ and the blue (printed in black) parts represent $\overline{\omega}_x' < -0.12u_\tau^2/\nu$. It can also be obtained that the finite-sized particles decrease the streamwise fluctuation intensities and make the structure different. Because of the particle concentrations in some special areas, particles make the streamwsie fluctuation distributions uneven.

CONCLUSIONS

Large-eddy simulations of the particle-laden rotating channel flows have been presented and compared with the single-phase flows at the Reynolds number Re=250 and the Rotation number Ro=0.0, 0.1, 0.25, 0.5, 1.0, and 1.5, respectively. Smagorinsky SGS model was applied in the calculations. From the simulations, we get the following conclusions.

lots of the particles concentrate near the pressure surface due to system rotation even at the low Rotation number in the fully-developed rotating turbulent channel flows. The turbulence intensities and their structures are changed by the Coriolis forces combined with the particle's concentrations, those phenomena are very obvious near two walls.

The inter-particle collisions will play an important role even at very low particle volume fractions $O(10^{-5})$ and change particle density distributions along the y direction. Finite-sized particles will attenuate the contributions of the Coriolis forces on the turbulence and the total turbulent kinetic energies of the carrier fluid in a rotating channel.

ACKNOWLEDGMENTS

The first author has been supported by the Japanese Government (Monbusho) scholarship, and we are also grateful for useful discussions with Dr. Y. Yamamoto.

REFERENCES

Bardina, J., Ferziger, J. & Rogallo, R.S., 1985, "Effect of Rotation on Isotropic Turbulence: Computation and Modelling," J. Fluid Mech., Vol. 154, pp. 321-336.

Bradshaw, P., 1969, "The Analogy between Streamline Curvature and Buoyancy in Turbulent Shear Flow," J. Fluid Mech., Vol.36, pp. 177-191.

Cambon, C., Benoit, J.P., Shao, L. & Jacquin, L., 1994, "Stability Analysis and Large-Eddy Simulation of Rotating Turbulence with Organized Eddies," J. Fluid Mech., Vol. 278, pp. 175-200.

Deardorff, J.W., 1970, "A Numerical Study of Three-dimensional Turbulent Channel Flow at Large Reynolds Numbers," J. Fluid Mech., Vol. 41(2), pp. 453-480.

Dennis, S.C.R., Singh, S.N. & Ingham, D.B., 1980, "The Steady Flow due to a Rotating Sphere at Low and Moderate Reynolds Number. J. Fluid Mech., Vol.101, pp.257-279.

Fessler, J. R., Kulick, J. D. & Eaton, J. K., 1994, "Preferential Concentration of Heavy Particles in a Turbulent Channel Flow," Phys. Fluids, Vol. 6, pp.3742-3749.

Howard, J.H.G., Patankar, S.V. & Bordynuik, R.M., 1980, "Flow Prediction in Rotating Ducts Using Coriolis-Modifed Turbulence Models," Trans. ASME I: J. Fluids Engng, Vol.102, pp.456-461.

Johnston, J.P., Halleen, R.M. & Lezius, D.K., 1972, "Effects of Spanwise Rotation on the Structure of Two-dimensional Fully Developed Turbulent Channel Flow," J. Fluid Mech., Vol.56, pp.533-557.

Kim, J., 1983, "The Effect of Rotation on Turbulence Structure," In Proc. 4th Symp. On Turbulent Shear Flows, Karsruhe, pp.6.14-6.19.

Kristoffersen, R. & Andersson, H.I., 1993, "Direct Simulations of Low-Reynolds-Number Turbulent Flow in a Rotating Channel," J. Fluid Mech., Vol. 256, pp.163-197.

Koyama, H., Masuda, S., Ariga, I. & Watanabe, I., 1979, "Stabilizing and Destabilizing Effects of Coriolis Force on Two-dimensional Laminar and Turbulent Boundary Layers," Trans. ASME A: J. Engng Power, Vol.101, pp.25-31.

Launder, B.E., Telepidakis, D.P. & Younis, B.A., 1987, "A Second-Moment Closure Study of Rotating Channel Flow," J. Fluid Mech., Vol.183, pp.63-75.

Maxey, M.R. & Riley, J.J., 1983, "Equation of Motion for a Small Rigid Sphere in Nonuniform Flow," Phys. Fluids. Vol.26, pp.883.

Miyake, Y. & Kajishima, T., 1986, "Numerical Simulation of the Effects of Coriolis Force on the Structure of Turbulence. Global effects," Bull. JSME, Vol.29,pp.3341-3346.

Piomelli, U. & Liu, J.-H., 1995, "Large-Eddy Simulation of Rotating Channel Flows Using a Localized Dynamic Model," Phys. Fluids, Vol.7 (4), pp.839-848.

Rouson, D.W.I. & Eaton, J.K. 1994, "Direct Numerical Simulation of Turbulent Channel Flow with Immersed Particles," ASME/FED Numerical Methods in Multiphase Flows (ed. Sommerfeld, M.), pp.185.

Saffman, P.G., 1965, "The Lift on a Small Sphere in a Slow Shear Flow," J. Fluid Mech., Vol.22(2), pp.385-400.

Schiller, L. & Nauman, A., 1933, *V. D. I.* Zeits, Vol.77, pp.318.

Tabakoff, W., 1984, "Review-Turbomachinery Performance Deterioration Exposed to Solid Particulates Environment," ASME J. Fluid Eng., Vol.106, pp.125-134.

Tafti, D.K. & Vanka, S.P., 1991, "A numerical Study of the Effects of Spanwise Rotation on Turbulent Channel Flow," Phys. Fluids, A Vol.3(4), pp.642-656.

Takagi, H., 1977, "Viscous Flow Induced by Slow Rotation of a Sphere," J. Phys. Soc. Japan, Vol.42, pp.319-325.

Tanaka, T. & Tsuji, Y., 1991, "Numerical Simulation of Gas-Solid Two-Phase Flow in a Vertical Pipe, on the Effect of Inter-Particle Collision," ASME/FED Gas-Solid Flows, pp.123-128.

Tsuji, Y., 1984, *Pneumatic Conveying*, Nikkann, Kogyo (in Japanese).

Wang, Q.Z. & Sqires, K.D., 1996, "Large-Eddy Simulation of Particle-Laden Turbulent Channel Flow," Phys. Fluids, Vol.8(5), pp.1207-1223.

Yamamoto, Y., Tanaka, T. & Tsuji, Y., 1998, "LES of Gas-Particle Turbulent Channel Flow (the Effect of Inter-Particle Collision on Structure of Particle Distribution)," Proceedings of the 3rd Intl. Conference on Multiphase Flow, pp.518.